Colloidal metal particles as probes of nanoscale thermal transport in fluids

Orla M. Wilson, Xiaoyuan Hu, David G. Cahill,* and Paul V. Braun
Department of Materials Science and Engineering, and the Frederick Seitz Materials Research Laboratory, University of Illinois, Urbana, Illinois 61801

(Received 8 August 2002; published 10 December 2002)

We investigate suspensions of 3–10 nm diameter Au, Pt, and AuPd nanoparticles as probes of thermal transport in fluids and determine approximate values for the thermal conductance G of the particle/fluid interfaces. Subpicosecond $\lambda = 770$ nm optical pulses from a Ti:sapphire mode-locked laser are used to heat the particles and interrogate the decay of their temperature through time-resolved changes in optical absorption. The thermal decay of alkanethiol-terminated Au nanoparticles in toluene is partially obscured by other effects; we set a lower limit $G > 20$ MW m^{-2} K^{-1}. The thermal decay of citrate-stabilized Pt nanoparticles in water gives $G \approx 130$ MW m^{-2} K^{-1}. AuPd alloy nanoparticles in toluene and stabilized by alkanethiol termination give $G \approx 5$ MW m^{-2} K^{-1}. The measured G are within a factor of 2 of theoretical estimates based on the diffuse-mismatch model.

DOI: 10.1103/PhysRevB.66.224301 PACS number(s): 66.60.+a, 68.65.−k, 68.08.−p, 81.07.−b

I. INTRODUCTION

Increasing interest in the transport of thermal energy on nanometer length scales is accompanying the shrinking scale of devices and emerging applications for nanocomposite and multilayer materials.[1,2] Experimental methods for characterization of nanometer-scale thermal transport are also advancing rapidly: time-resolved thermoreflectance provides high spatial and temporal resolution to the one-dimensional flow of heat from the surface of a metal film;[3] micromachined test structures[4] and scanning thermal microscopies[5] are used to examine heat flow in nanowires; and high resolution lithography enables measurements of heat flow in semiconductor device structures.[6] Here, we describe our initial experiments on the use of colloidal metal particles as probes of the nanometer scale thermophysical properties of fluids and solid-fluid interfaces. We believe our results will impact more applied efforts at developing and understanding novel heat transfer fluids,[7] targeted thermal effects in medical therapies,[8,9] and photothermally activated drug delivery.[10]

For sufficiently small particles, the thermal conductance per unit area G of the particle-fluid interface will play an important role in the thermal decay of a particle heated by a laser pulse. In the absence of interface effects $G \to \infty$, the characteristic time τ_d for the cooling of a spherical particle can be estimated by equating the heat capacity of the particle to the heat capacity of a layer of the surrounding fluid with the thickness of the thermal diffusion length $l_d = \sqrt{D_f \tau_d}$; $\frac{4}{3}\pi r^3 C_p = 4\pi r^2 l_d C_f$, where C_p and C_f are the heat capacities per unit volume of the particle and the fluid, respectively, and r is the particle radius. Therefore,

$$\tau_d = \frac{r^2 C_p^2}{9 C_f \Lambda_f}, \tag{1}$$

where Λ_f is the thermal conductivity of the fluid. Alternatively, if the cooling of the nanoparticle is controlled by the interface thermal conductance, then the cooling time is given by the ratio of the heat capacity of the particle to the total thermal conductance of the particle-fluid interface

$$\tau_i = \frac{r C_p}{3G}. \tag{2}$$

Setting $\tau_d = \tau_i$, defines a critical value of G

$$G_c = \frac{3 C_f \Lambda_f}{r C_p}. \tag{3}$$

With $G \gg G_c$, the cooling of the nanoparticle is controlled by the effusivity of the fluid $\Lambda_f C_f$. With $G \ll G_c$, the cooling is controlled by the interface thermal conductance G. For an $r = 5$ nm particle in an organic solvent such as toluene $G_c \approx 50$ MW m^{-2} K^{-1}; the same particle in water gives $G_c = 600$ MW m^{-2} K^{-1}. We are not aware of any previous quantitative studies of G for solid-liquid interfaces but reported values[11,12] for the thermal conductance of solid-solid interfaces span a similar range $30 < G < 700$ MW m^{-2} K^{-1}. The thermal conductance of Cu interfaces with liquid He—usually discussed in terms of the inverse of G, the Kapitza resistance—has been thoroughly studied[13] but we cannot extrapolate these results and predict the behavior of classical fluids at room temperature.

The decay of electronic excitations of nanoparticles measured by pump-probe laser spectroscopies has an extensive literature.[14–18] Thermal decays at longer-time scales have also been observed but have typically been a secondary consideration.[19–22] (A notable exception is the recent work by Hu and Hartland[23] who showed that the decay time of citrate-stabilized Au nanoparticles varied from 10 to 380 ps as the particle radius was varied from 5 to 50 nm.) In the majority of the prior work, the pump excitation is produced by the frequency doubled $\lambda = 390$ nm light from a regeneratively amplified Ti:sapphire laser. Typically, the temperature of the metal nanoparticle is inferred through changes in optical absorption of the particle-fluid mixture measured by a time-delayed probe beam; changes in the real part of the index of refraction are also accessible through transient lensing[22] of the probe beam or probe beam refraction.[24] At low particle densities, the complex index of refraction of the

particle-fluid mixture is a simple function of the dielectric constants of the nanoparticle and fluid.[25]

To minimize the temperature excursions of the nanoparticles and possible photochemical damage to our samples, we limit our studies to excitation and detection using pulses of near infrared light generated by a mode-locked Ti:sapphire laser. This approach simplifies the experiments and enables high modulation frequencies that minimize laser noise. We avoid the need for flow cells or large sample volumes; a full sample cell in our apparatus requires <2 μL of fluid.

II. EXPERIMENTAL DETAILS

A. Nanoparticle synthesis

(a) *Thiol-stabilized Au, d = 3 nm.* Au nanoparticles were synthesized following the method of Brust *et al.*[26] $HAuCl_4$ (30 mL, 30 mM) was transferred from an aqueous to a toluene phase using tetraoctylammonium bromide (TOABr) in toluene (80 mL, 50 mM) as the phase-transfer agent. The organic layer was separated, and dodecanethiol (DodSH) (170 mg, 0.84 mmoles) was added under vigorous stirring. A large excess of aqueous sodium borohydride (25 mL, 0.4 M) was then added dropwise and the mixture was stirred for 3 h at room temperature. The organic phase was collected, concentrated to 10 mL by rotary evaporation, and precipitated twice from excess ethanol (30:1) overnight in a freezer.

(b) *Thiol-stabilized Au, d=5 nm.* Larger Au nanoparticles were synthesized by increasing the Au:DodSH ratio as described by Leff *et al.*[27] (i) 3.5:1 (Au:RSH). $HAuCl_4$ (15 mL, 30 mM) was transferred to toluene with TOABr (10.2 mL, 100 mM). After the addition of DodSH in toluene (3.13 mL, 40 mM), $NaBH_4$ (12.5 mL, 0.4M) was added dropwise with vigorous stirring. The reaction mixture was stirred overnight and the product was precipitated twice from ethanol as described above. (ii) 5.0:1 (Au:RSH). A solution of $HAuCl_4$ (7.5 mL, 89 mM) was mixed with TOABr in toluene (15 mL, 100 mM). After the addition of DodSH in toluene (3.19 mL, 40 mM) to the organic phase, $NaBH_4$ (18 mL, 0.4 M) was added dropwise with vigorous stirring. After stirring the reaction mixture overnight, the product was precipitated twice from ethanol.

(c) *Thiol-stabilized AuPd, d=10 nm.* AuPd alloy nanoparticles were produced by co-reduction of $PdCl_2$ and $HAuCl_4$ in a Brust-type synthesis. For $Au_{0.94}Pd_{0.06}$, aqueous $PdCl_2$ (5 mL, 10 mM) was added to a vigorously stirred solution of $HAuCl_4$ (25 mL, 30 mM). Phase-transfer to toluene was carried out with TOABr (80 mL, 25 mM), and DodSH (170 mg, 0.84 mmol) was added to the organic phase. Reduction took place following dropwise addition of $NaBH_4$ (20 mL, 0.5 M) and the mixture was left stirring for 3 h. Initial cleaning of the product was carried out as described above. In addition to removal of excess reactants by precipitation from ethanol, the polydispersity was decreased by the use of size-selective precipitation.[28] Acetone, a nonsolvent, was added by passive vapor transfer to a concentrated colloidal dispersion of the AuPd particles in toluene. After 2 days, the supernatant was removed and the process was repeated on both the sediment and supernatant. The second supernatant showed a much-decreased polydispersity and this sample was used for studies of thermal transport.

(c) *Citrate-stabilized Pt, d=10 nm.* Pt nanoparticles were prepared by hydrogen reduction following the procedures described by Henglein and co-workers.[29–31] A K_2PtCl_4 aqueous solution (10 mM) was prepared using double distilled water and aged for 4 days before reduction. (The reduction of aged solution of $PtCl_4^{2-}$ is much faster than that of freshly prepared solution due to the formation of hydrate.[29]) The solution was diluted to ≈ 0.5 mM and sodium citrate (0.2 mM) was added as a stabilizer to prevent agglomeration. The solution was flushed with nitrogen for 20 min. Then, pure hydrogen was introduced into the system and bubbled vigorously for 3 min. The vessel was subsequently sealed to allow the reaction to complete. The vessel was occasionally shaken to ensure saturation of the solution with hydrogen. The solution was yellowish brown 5 min after H_2 introduction and turned black after two hours.

B. Transmission electron microscopy

Nanoparticle shapes, sizes, and size distributions are evaluated by transmission electron microscopy, see Fig. 1, using either a Philips CM12 or JEOL 2010 LaB6 microscope with accelerating voltages of 120 or 200 kV, respectively. The nanoparticle suspensions were dispensed on carbon-coated copper grids (Au and AuPd particles) or SiO_2-coated grids (Pt particles). Pt particles show pronounced faceting, see Fig. 1(b). Planar crystal defects are clearly visible in the AuPd alloy particles through diffraction contrast, see Fig. 1(c). In disagreement with the conclusions of Ref. 27, we did not observe significant differences in the average diameters of thiol-stabilized Au nanoparticles synthesized with 3.5:1 and 5:1 Au:RSH ratios (data not shown). In both cases, the average diameter was $d \approx 5$ nm.

C. Picosecond transient absorption

For transient absorption measurements, we use a mode-locked Ti:sapphire laser that produces a series of ≈ 0.15 ps pulses at a repetition rate of 80.6 MHz. The laser output is split into a ''pump'' beam and a ''probe'' beam whose relative optical path lengths are adjusted via a mechanical delay stage. We modified our thermoreflectance apparatus[2] to accommodate transmission measurements. A 20 mm focal-length microscope objective focuses the pump and probe beams and also forms a reflected-light dark-field microscopy image of the sample cell on a CCD camera.[32,2] The fluid cells are 0.1×1 mm^2 or 0.2×2 mm^2 flat-sided capillary tubes that are epoxied to a steel disk that serves as a heat sink and sample holder. We use pump and probe beam powers of 2–8 mW, a wavelength of 770 nm, and a $1/e^2$ beam radius of 8.5 μm. The energy density of the optical pulses is <0.2 mJ cm^{-2}. The differences in transmitted probe intensity caused by the pump pulse appear at the $f=9.8$ MHz modulation frequency of the pump beam and are extracted with lock-in detection.[32] The electro-optic modulator broadens the pump pulse to a width of ≈ 0.5 ps.

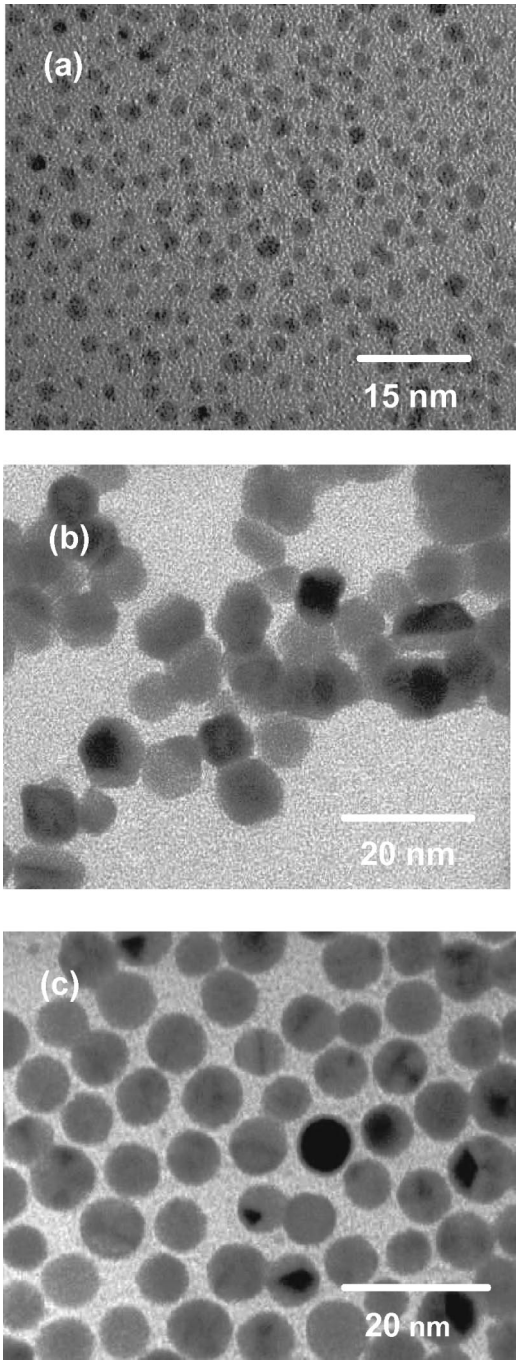

FIG. 1. Transmission electron micrographs of colloidal metal particles used in our studies of nanoscale thermal transport: (a) alkanethiol-terminated Au nanoparticles, average diameter $d=3$ nm; (b) citrate-stabilized Pt, $d=10$ nm; (c) alkanethiol-terminated AuPd alloys, $d=10$ nm. The nominal composition of the AuPd alloys is $Au_{0.94}Pd_{0.06}$.

D. Modeling of heat flow

Working in the frequency domain, we write three equations for the temperature of the nanoparticle T_p, the boundary condition at the interface, and the boundary condition on the temperature of the fluid T_f adjacent to the interface. The temperature gradient within the particle is negligible:

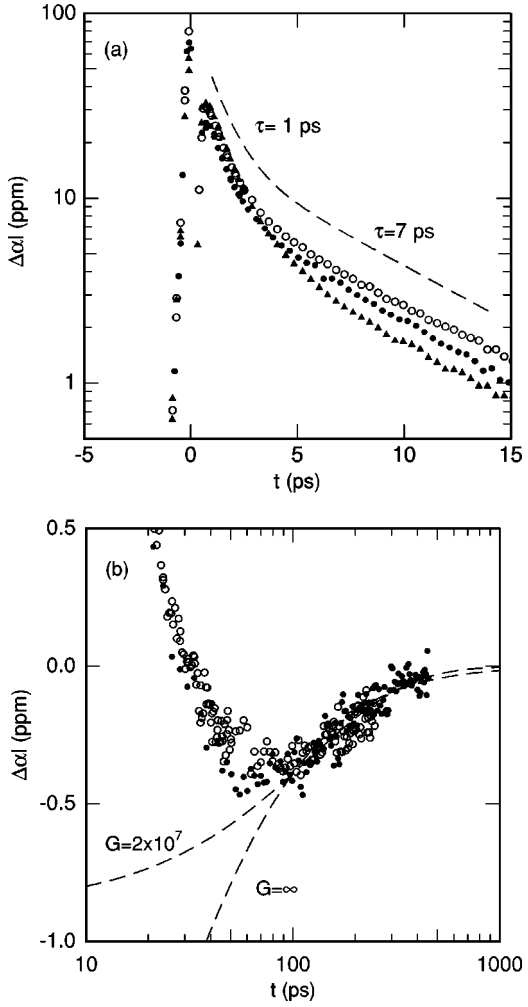

FIG. 2. Transient changes in optical absorption at (a) short times and (b) long times from suspensions of alkanethiol terminated Au nanoparticles in toluene: 3 nm diameter (solid triangles), 5 nm diameter (3.5:1 open circles, 5:1 solid circles). The pump and probe powers are ≈ 8 mW; the sample path length $l=0.1$ mm; and the absorption length $\alpha^{-1}\approx 5$ mm. The vertical scale is approximate. In (a), a two time-constant exponential decay (dashed line) is shown for comparison. In (b), calculated thermal decays, see Eqs. (4)–(8), are shown as dashed lines; the vertical scale of the theoretical curves are fit to the data at $t=100$ ps. The calculated decays are labeled by the thermal conductance G of the particle-fluid interface: $G=\infty$ excludes interface effects; $G=20$ MW m^{-2} K^{-1}is the lower limit on G that is consistent with the data.

$$\frac{4\pi}{3} i\omega r^3 C_p T_p = P - 4\pi r^2 F, \tag{4}$$

$$G(T_p - T_f) = F, \tag{5}$$

$$rF = T_f(1+qr)\Lambda_f. \tag{6}$$

P is the laser power that heats the nanoparticle, F is the heat flux at the particle-fluid interface, and $1/|q|$ is the thermal diffusion length in the fluid: $q^2 = i\omega/D_f$, $D_f = \Lambda_f/C_f$. We solve for T_p by eliminating F and T_f. For small temperature excursions, changes in optical absorption of the probe

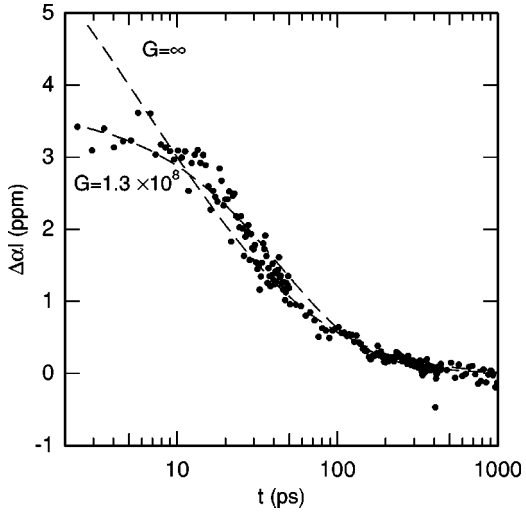

FIG. 3. Transient changes in optical absorption from suspensions of citrate-stabilized Pt nanoparticles in water; the average particle diameter is 10 nm. The pump and probe powers are ≈2 mW; the sample path length $l=0.1$ mm; and the absorption length α^{-1} ≈15 mm. Calculated thermal decays are shown as dashed lines; the vertical scale of the theoretical curves are adjusted to fit the data in the vicinity of $t=40$ ps. The calculated decays are labeled by the thermal conductance G of the particle-water interface. The units of G are W m^{-2} K^{-1}.

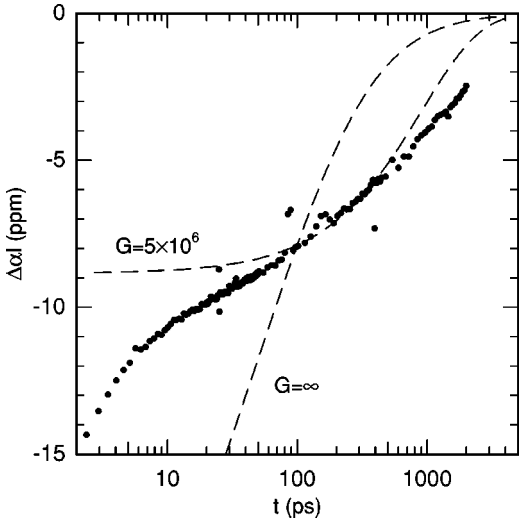

FIG. 4. Transient optical absorption from suspensions of alkanethiol terminated AuPd alloy nanoparticles in toluene; the average particle diameter is 10 nm. The pump and probe powers are ≈5 mW; the sample path length $l=0.2$ mm. Calculated thermal decays are shown as dashed lines; the vertical scale of the theoretical curves are fit to the data at $t=100$ ps. The calculated decays are labeled by the thermal conductance G of the particle-fluid interface. The units of G are W m^{-2} K^{-1}.

beam will be a linear function of the particle temperature; the in-phase signal of the lock-in amplifier is then[2]

$$S(q)=T_p(q/\tau+f)+T_p(q/\tau-f), \tag{7}$$

$$V_{\text{in}}(t)=A\sum_{q=-\infty}^{\infty} S(q)\exp(i2\pi tq/\tau), \tag{8}$$

where τ is the time between pulses, t is the time delay between pump and probe, and A is a constant.

III. RESULTS

In Fig. 2, we plot the transient change in optical absorption measured for alkanethiol terminated Au nanoparticles. At short times, the transmission decreases quickly with a $\tau=1$ ps time constant and then more slowly with $\tau=7$ ps. We can assign the first decay to the cooling of the Au electron gas. In bulk Au, the decay time of the electron gas for small temperature excursions near room temperature is predicted[33,34] to be $\tau=0.7$ ps, in good agreement with our results and prior measurements of electron dynamics in Au nanoparticles in the limit of low-energy laser pulses.[15] (Often, the cooling time of the electron gas is confused with the electron-phonon scattering time. In Au at room temperature, the electron-phonon scattering time is 25 times smaller than the cooling time.[33])

We do not understand the origin of the $\tau=7$ ps decay. The fastest possible decay of the temperature of the Au lattice should have a characteristic time scale given by Eq. (1), $\tau_d=110$ ps for $r=5$ nm, and furthermore, in this limit of $G\rightarrow\infty$ the temperature would not decay exponentially with time. We speculate that the $\tau=7$ ps signal arises from an electronic effect associated with the Au-alkanethiol interfaces. Structural relaxations of the alkanethiol termination are a more remote possibility. We observed essentially the same signal using probe-beam refraction (data not shown) in samples of lower optical density.

The electronic signals in pure Au nanoparticles mostly obscure the thermal decay for our choice of pump and probe wavelengths $\lambda=770$ nm. Nevertheless, the tail of the data shown in Fig. 2(b) allows us to set a lower limit on G for these samples, $G>20$ MW m^{-2} K^{-1}.

Our data for citrate-stabilized Pt nanoparticles in water are in good agreement with the thermal decays of similarly sized citrate-stabilized Au particles measured by Hu and Hartland.[23] (The authors of Ref. 23 did not consider interface conductance in their analysis.) The electronic signal (data not shown) in Pt nanoparticles is negligible at $t>2$ ps. Thus the thermal decay can be followed at much shorter delay times than is possible in Au. The best fit to the data gives $G\approx130$ MW m^{-2} K^{-1}, see Fig. 3.

To overcome the weak thermal signals of pure Au nanoparticles, we developed AuPd alloy nanoparticles. The addition of Pd is intended to increase the optical absorption and the temperature dependence of the optical constants at $\lambda=770$ nm. The results for a nominal composition of $Au_{0.94}Pd_{0.06}$ are shown in Fig. 4. In pure Au, the thermal signal does not dominate the measurement until $t>100$ ps; in AuPd, the thermal signal dominates for $t>10$ ps and so a much larger range of delay times can be compared with theory. We extract $G\approx5$ MW m^{-2} K^{-1}. Since $G\ll G_c$, the predicted decay is exponential with a time constant $\tau_i=820$ ps.

The fit between the data and this single time-constant ex-

ponential decay is, however, far from perfect. The decay time depends on the ratio r/G, see Eq. (2). Polydispersity in r does not appear to be sufficient to explain the discrepancies at short and long times; we conclude that polydispersity of G is more significant and creates the more gradual decay seen in the data in Fig. 4.

IV. DISCUSSION AND CONCLUSIONS

To gain physical insight, we compare our results to theoretical estimates based on the diffuse-mismatch model (DMM).[13] The DMM was originally developed to aid understanding of the thermal conductance of solid-solid interfaces. In the simplest implementation of the DMM, the Debye model is used to describe the vibrational density of states on both sides of the interface. Phonons are assumed to be randomly and elastically scattered at the interface with a transmission coefficient given by the ratio of the phonon densities of states. The DMM often overestimates G for solid-solid interfaces near room temperature[11] but we have recently shown that the DMM is in excellent agreement with data for epitaxial TiN/MgO and TiN/Al_2O_3 interfaces of high quality.

While phonons are probably well defined in our $d > 5$ nm Pt or Au nanoparticles, only the low-frequency longitudinal vibrational modes of H_2O and toluene are wavelike. But lacking any other analytical approach, we examine the DMM predictions for Pt/H_2O and Au/toluene using a Debye density of states in the fluids with a transverse speed of sound that is 60% of the longitudinal speed of sound $v_t = 0.6v_l$. We do not consider the intramolecular vibrations and treat each molecule as a rigid unit. These calculations give $G_{\mathrm{DMM}} = 62$ MW m^{-2} K^{-1} for the Pt/H_2O interface and $G_{\mathrm{DMM}} = 12$ MW m^{-2} K^{-1} for Au/toluene. Thus, despite all the shortcomings and approximations of the DMM, the predicted G_{DMM} fall within a factor of ≈ 2 of our measurements. Quantitative modeling of G may require more sophisticated approaches such as molecular dynamics simulation.

AuPd alloy nanoparticles appear to be particularly well suited for further systematic study: the transient optical absorption signals are large, stable, and easily measured. We expect that changes in interface chemistry or composition will produce significant changes in G and enable rigorous tests of theoretical models.

ACKNOWLEDGMENTS

This work was supported by U.S. DOE Grant No. DE-FG02-01ER45938. The Ti:sapphire laser is part of the Laser Facility of the Seitz Materials Research Laboratory at the University of Illinois. TEM characterization of the colloidal particles was carried out in the Center for Microanalysis of Materials, University of Illinois, which is partially supported by the U.S. Department of Energy under Grant No. DEFG02-96-ER45439.

*Electronic address: d-cahill@uiuc.edu

[1] D. G. Cahill, W. K. Ford, K. E. Goodson, G. D. Mahan, A. Majumdar, H. J. Maris, R. Merlin, and S. R. Phillpot, J. Appl. Phys. **93**, 1 (2002).
[2] D. G. Cahill, K. E. Goodson, and A. Majumdar, J. Heat Transfer **124**, 223 (2002).
[3] W. S. Capinski, H. J. Maris, T. Ruf, M. Cardona, K. Ploog, and D. S. Katzer, Phys. Rev. B **59**, 8105 (1999).
[4] P. Kim, L. Shi, A. Majumdar, and P. L. McEuen, Phys. Rev. Lett. **87**, 215502 (2001).
[5] A. Majumdar, Annu. Rev. Mater. Sci. **29**, 505 (1999).
[6] P. G. Sverdrup, S. Sinha, M. Asheghi, U. Srinivasan, and K. E. Goodson, Appl. Phys. Lett. **78**, 3331 (2001).
[7] J. A. Eastman, S. U. S. Choi, S. Li, W. Yu, and L. J. Thompson, Appl. Phys. Lett. **78**, 718 (2000).
[8] G. Hüttmann and R. Birngruber, IEEE J. Sel. Top. Quantum Electron. **5**, 954 (1999).
[9] K. Hamad-Schifferil, J. J. Schwartz, A. T. Santos, S. Zhang, and J. M. Jacobson, Nature (London) **415**, 152 (2002).
[10] J. L. West and N. J. Halas, Curr. Opin. Biotechnol. **11**, 215 (2000).
[11] R. J. Stoner and H. J. Maris, Phys. Rev. B **48**, 16 373 (1993).
[12] R. M. Costescu, M. A. Wall, and D. G. Cahill (unpublished).
[13] E. T. Swartz and R. O. Pohl, Rev. Mod. Phys. **61**, 605 (1989).
[14] J.-Y. Bigot, J.-C. Merle, O. Cregut, and A. Daunois, Phys. Rev. Lett. **75**, 4702 (1995).
[15] J. Hodak, I. Martini, and G. V. Hartland, Chem. Phys. Lett. **284**, 135 (1998).
[16] S. Link, C. Burda, Z. L. Wang, and M. A. El-Sayed, J. Chem. Phys. **111**, 1255 (1999).
[17] V. Halté, J.-Y. Bigot, B. Palpant, M. Broyer, B. Prével, and A. Pérez, Appl. Phys. Lett. **75**, 3799 (1999).
[18] J. H. Hodak, A. Henglein, and G. V. Hartland, J. Chem. Phys. **114**, 2760 (2001).
[19] T. W. Roberti, B. A. Smith, and J. Z. Zhang, J. Chem. Phys. **102**, 3860 (1995).
[20] M. Perner, P. Bost, U. Lemmer, G. von Plessen, J. Feldmann, U. Becker, M. Mennig, M. Schmitt, and H. Schmidt, Phys. Rev. Lett. **78**, 2192 (1997).
[21] H. Inouye, K. Tanaka, I. Tanahashi, and K. Hirao, Phys. Rev. B **57**, 11 334 (1998).
[22] A. Harata, J. Taura, and T. Ogawa, Jpn. J. Appl. Phys. **39**, 2909 (2000).
[23] M. Hu and G. V. Hartland, J. Phys. Chem. **106**, 7029 (2002).
[24] S. E. Bialkowski, *Photothermal Spectroscopy Methods For Chemical Analysis*, Vol. 134 of *Chemical Analysis* (Wiley-Interscience, New York, 1996).
[25] P. Mulvaney, Langmuir **12**, 788 (1996).
[26] M. Brust, M. Walker, D. Bethell, D. J. Schiffrin, and R. Whyman, J. Chem. Soc. Chem. Commun. **1994**, 801.
[27] D. V. Leff, P. C. O'Hara, J. R. Heath, and W. M. Gelbart, J. Phys. Chem. **99**, 7036 (1995).
[28] R. L. Whetten, J. T. Khoury, M. M. Alvarez, S. Murthy, I. Vezmar, Z. L. Wang, P. W. Stephens, C. L. Cleveland, W. D. Luedtke, and U. Landman, Adv. Mater. **8**, 428 (1996).
[29] A. Henglein, B. G. Ershov, and M. Malow, J. Phys. Chem. **99**, 14 129 (1995).
[30] T. S. Ahmadi, Z. L. Wang, T. C. Green, A. Henglein, and M. A. El-Sayed, Science **272**, 1924 (1996).

[31] A. Henglein and M. Giersig, J. Phys. Chem. B **104**, 6767 (2000).
[32] K. E. O'Hara, X.-Y. Hu, and D. G. Cahill, J. Appl. Phys. **90**, 4852 (2001).
[33] P. B. Allen, Phys. Rev. Lett. **59**, 1460 (1987).
[34] S. D. Brorson, A. Kazeroonian, J. S. Moodera, D. W. Face, T. K. Cheng, E. P. Ippen, M. S. Dresselhaus, and G. Dresselhaus, Phys. Rev. Lett. **64**, 2172 (1990).